# $WSe_2$ thin-film realization by synthesis and by tarnishing



1994 J. Phys.: Condens. Matter 6 8527

(http://iopscience.iop.org/0953-8984/6/41/015)

J. Phys.: Condens. Matter 6 (1994) 8527–8537. Printed in the UK

# $WSe_2$ thin-film realization by synthesis and by tarnishing

A Khelil†, H Essaidi‡, J C Bernède‡, A Bouacheria† and J Pouzet‡

† Laboratoire de Physique des Matériaux et Composants pour l'Electronique, Université d'Oran Es Sénia, BP 1642 Oran, Algeria

‡ Laboratoire de Physique des Matériaux pour l'Electronique, Université de Nantes, 2 rue de la Houssinière, 44072 Nantes Cédex 03, France

Received 26 May 1994, in final form 1 August 1994

**Abstract.** Thin W films were deposited by RF sputtering onto a glass substrate and then covered with an Se layer. The $WSe_2$ layers were obtained either by annealing the W layers in a vacuum sealed Pyrex tube or by the tarnishing reaction of Se vapour on W films. The properties of the thin $WSe_2$ films made by synthesis and by tarnishing are described. The layers were examined by x-ray diffraction, x-ray photoelectron spectroscopy, scanning and transmission electron microscopy, electron microprobe analysis, optical transmission and resistivity measurements.

The films crystallize in the hexagonal structure. It has been found that stoichiometric layers are obtained after synthesis while layers obtained by tarnishing are partly oxidized. The optical gap of the synthesized layers is in good agreement with the expected value. The electrical resistance is governed by grain boundary scattering mechanisms.

## 1. Introduction

Tungsten diselenide ($WSe_2$) is a semiconductor that can act as efficient electrodes in the realization of photoelectrochemical solar cells [1]. For economic reasons, obtaining $WSe_2$ in thin films would be interesting.

We have already described a very simple process to obtain $WSe_2$ films by soft selenization of W [2]. $WSe_2$ layers were synthesized by annealing, under Se pressure, RF sputtered W films deposited onto a glass substrate. The Se needed for the growth of $WSe_2$ during the annealing in the vacuum sealed Pyrex tube was provided by the insertion of a small amount of Se powder into the tube before sealing.

In this paper we describe the properties of thin films obtained by two different techniques:

(i) the first one consists of an improvement of the process briefly recalled above;
(ii) the second one is called tarnishing [3] and will be developed below.

The properties of $WSe_2$ obtained by these two low-temperature processes are compared. The preparation and the structural, morphological and chemical characterization of these films will be described. The electrical properties will also be presented.

## 2. Experimental details

### 2.1. *First process*

W thin films of thicknesses between 280 and 320 nm were deposited by RF sputtering on a glass substrate [2]. Then without breaking the vacuum Se thin films of thickness of about

0953-8984/94/418527+11$19.50  

0.9 $\mu$m were deposited. The Se thickness is sufficient that no more Se is needed during the process, which avoids the wasting of Se that was unavoidable in the process described above. After thin-film deposition the samples were placed in a vacuum sealed Pyrex tube and heated to temperatures between 773 and 823 K for 48–120 h.

Early works [2] have shown that some Se condensation takes place on the surface of the layers during the cooling of the Pyrex tube. Therefore this excess is sublimated by annealing the samples under dynamic vacuum for 24 h at $T = 675$ K.

### 2.2. *Second process*

The same layers as in the first process were deposited; however here the Se layer is just a capping layer used to protect the W film from oxidation and it is thinner ($\sim$ 50 nm) than in the first process. Then the samples were reacted in an open quartz furnace. Recently [4], $WS_2$ has been obtained by a similar process. However sulphur powder is not used as the chalcogen source but a flow of $H_2S$ with forming gas 5%$H_2$, 95%$N_2$. For safety reasons we have not worked with $H_2Se$ but with Se powder as the chalcogen source. A constant flow of Ar (6 l $h^{-1}$) was maintained to remove $O_2$, in order to try to avoid oxidation during the process. The W layers were situated in the hot zone of the reactor (673 K $< T <$ 823 K) while the Se source was heated to 575 K.

The temperatures in the reactor were measured by chromel–alumel thermocouples. The reaction in the reactor may be written $W_{(s)} + Se_{2(g)} \rightarrow WSe_{2(s)}$. After the furnace reached the desired temperatures and a uniform gas flow was maintained, the samples were introduced into the reactor for times between 1 h and 4 h. After reaction the samples were moved back to the cold zone of the reaction chamber.

The layers obtained by the two processes were characterized by x-ray diffraction (XRD), x-ray photoelectron spectroscopy (XPS), electronic microscopy and electrical and optical measurements.

The structure of the films was examined using an x-ray diffractometer. The grain size $d$ was estimated from the full width at half maximum (FWHM) of the diffraction peaks [5, 6]. The degrees of preferential orientation $F(0, 0, l)$ and $F(h, k, 0)$, i.e. crystallites with the $c$ axis perpendicular and parallel to the plane of the substrate respectively, were estimated from the formula given by Janda and Kubovy [7].

XPS measurements were performed with an Mg x-ray source (1253 eV) operating at 10 kV and 10 mA at the University of Nantes. Data acquisition and treatment are realized through a computer and a standard programme. The quantitative studies were based on the determination of the W 4f and Se 3d peak areas with 2.14 and 0.57 respectively as sensitivity factors (the sensitivity factors of the spectrometer are given by Leybold, the manufacturer). The substrate being insulating ($10 \times 11 \times 1$ $mm^3$), the samples were earthed with Ag paste. The depth profiling was traced by recording successive x-ray photoelectron spectra obtained after Ar ion sputtering for short periods. Sputtering was accomplished at pressures of less than $5 \times 10^{-3}$ Pa with a 10 mA emission current and a 3 kV beam energy using an ion gun. The $Ar^+$ beam could be rastered over the entire sample surface. Before sputtering, the pressure was better than $5 \times 10^{-6}$ Pa.

Detailed morphological analysis of the films was carried out by scanning electron microscopy (SEM) using a Jeol 6400F field emission electron microscope. Another electron microscope equipped with a microprobe analyser was used to check the composition of the films. Transmission electron microscopy (TEM) and electron diffraction were used to control the orientation, homogeneity and morphology of the deposits. For examination in the TEM, the films were chemically removed from the glass substrates and then attached to Cu grids.

Electrical measurements were performed on planar samples. Evaporated Au was used in order to deposit electrodes on the planar structures. Cu wire was attached to the Au with Ag paste.

The DC conductance of the structures was measured by an electrometer. During measurements the currents generated by the electrometer were between 1 nA (2 GΩ) and 1 μA (2 MΩ). Electrical measurements were carried out in the dark between 80 and 500 K. Au gives a good ohmic contact, the layers obtained being p type semiconducting as shown by the classical hot-probe technique.

The optical measurements were carried out at room temperature using a Cary spectrophotometer. The optical density was measured at wavelengths from 2 to 0.4 μm. The absorption coefficient $\alpha$ has been calculated from the transmission $T$ and from the single-crystal surface reflectivity $R_0 \simeq 0.35$ [8]. Since in the spectral regions of interest in this work, i.e. at energies below the A exciton, the optical dispersion is small and the surface reflectivity has been taken to be effectively constant. Any errors incurred in the values of $R_0$ cause uncertainties in $\alpha$ that are much less than the errors in the thickness measurements that dominate the experimental errors [9]: $T \simeq (1 - R_0)^2 \exp(\alpha d)$, where $d$ is the thin-film thickness. The indirect energy gap is determined by extrapolating different plots of $\alpha = K(h\nu - E_0)^n$ to zero absorption, $K$ being a constant, $h$ the Planck constant and $\nu$ the frequency; $n$ can be anywhere in the range 1–2, $WSe_2$ being a layered indirect band gap semiconductor [10]. The thicknesses are measured by interferometry.

## 3. Results

### *3.1. Physicochemical characterization*

The W layer after deposition was found by XRD to be amorphous. In order to study systematically the crystallization (grain size orientation) the annealing time ($t_1$) and temperature ($T_1$) were varied.

As shown by XPS analysis and electron microprobe analysis, the atomic concentrations of the elements were found to be in good agreement with the $WSe_2$ stoichiometry and did not depend on the heat treatment conditions within the experimental error of these techniques (1–2 at.%).

However the O contamination of the layers was studied by recording successive x-ray photoelectron spectra obtained before and after Ar ion etching. While in films obtained by the first process, after 3 min of etching the O is not quantifiable, in the films obtained by the second process there is always 10–20 at.% O.

These results are confirmed by XRD spectra. Reproducible results are obtained only when $T \geqslant 823$ K and not less. After reaction, films of $WSe_2$ in the hexagonal structure have been obtained (figure 1). It can be seen in figure 1($a$) that only $WSe_2$ peaks are visible in the synthesized layers while extra peaks are detected in the layers obtained by tarnishing. These peaks may be attributed to $WO_3$. The presence of oxide in the films is also visible on the x-ray photoelectron spectra of W 4f (figure 2). The shape of the W 4f signal can be attributed to two doublets superimposed, the two W $4f_{5/2}$ peaks being at 33.35 and 30 eV, which correspond to $WO_3$ and $WSe_2$.

Therefore x-ray analysis has been used to estimate the size of the grains and the texture of the layers only for synthesized layers. The grain size estimated from the FWHM method is between 30 nm and 80 nm (table 1). Table 1 also shows $F(hk0)$ and $F(00l)$ for different annealing conditions. $F(00l)$, i.e. the texture of the films with the $c$ axis of the crystallites perpendicular to the plane of the substrate, increases with annealing time.

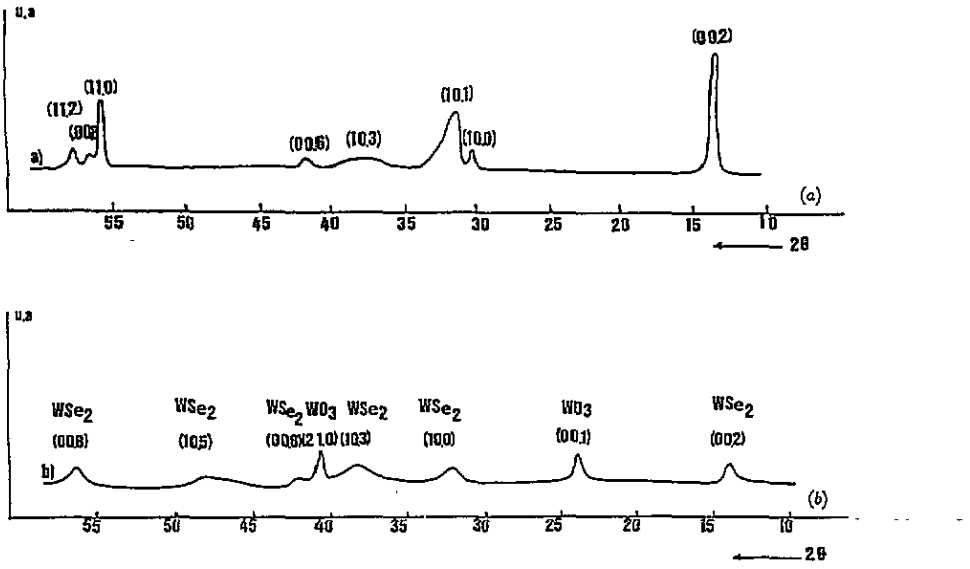


**Figure 1.** XRD patterns (Cu K$\alpha$ radiation) of $WSe_2$ layers obtained by (*a*) synthesis ($t_1 = 48$ h, $T_1 = 823$ K) and (*b*) tarnishing ($t = 5$ h, $T = 800$ K).

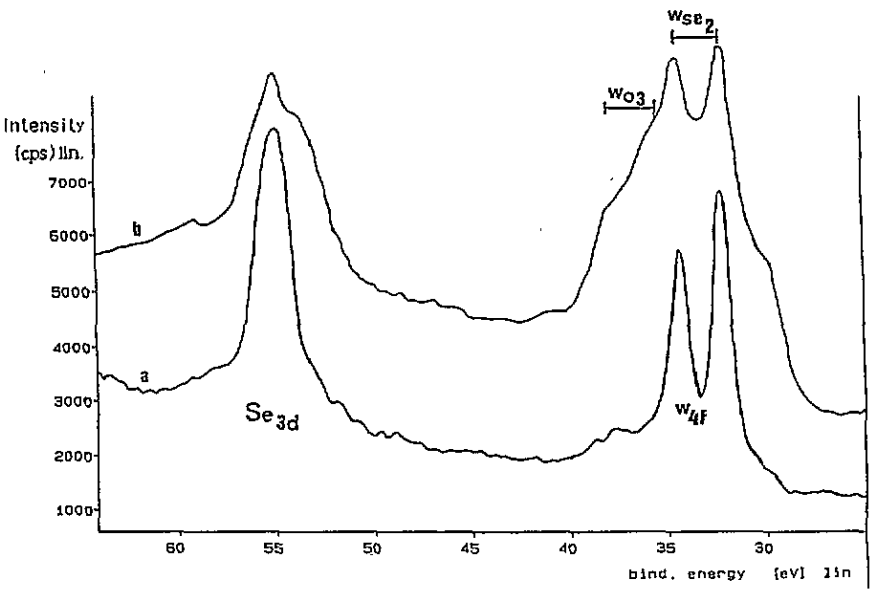


**Figure 2.** X-ray photoelectron spectra of W 4*f* and Se 3d after 3 min sputtering of $WSe_2$ layers obtained by synthesis ($t_1 = 48$ h, $T_1 = 823$ K (curve a) and tarnishing ($t = 5$ h, $T = 800$ K) (curve b)).

The $d_{hkl}$ values deduced from XRD patterns are in good agreement with those expected within the experimental error range (table 2). The *c* axis lattice constant was determined using the (002) spacing (table 2). Again there is a good agreement with the ASTM value

**Table 1.** Crystalline orientations and grain sizes deduced from XRD patterns of synthesized $WSe_2$ layers.

| Samples | Annealing conditions | | Crystalline orientations | | Grain size | | Thickness |
|---|---|---|---|---|---|---|---|
| | Duration (h) | Temperature (K) | $F(0,0,l)$ | $F(h,k,0)$ | $d_{\parallel c}$ (nm) | $d_{\perp c}$ (nm) | $e$ (nm) |
| $V_4$ | 48 | 823 | 0.2 | 0.4 | 48 | 55 | 900 |
| $V_6$ | 48 | 823 | 0.4 | 0.2 | 55 | 67 | 850 |
| $V_7$ | 48 | 823 | 0.7 | 0.1 | 62 | 82 | 900 |
| $V_{13}$ | 120 | 823 | 0.7 | 0.1 | 48 | 62 | 900 |
| $V_{16}$ | 120 | 823 | 0.8 | 0.1 | 29 | 54 | 900 |

[5]. Then the $a$ axis lattice constant was determined by using the (100) spacings (table 2). Here also there is good agreement with the ASTM value.

The results obtained by TEM analysis are shown in figure 3. Figure 3($b$) shows a bright-field image. We clearly see a closely packed structure of crystallites with many defects. However crystals with their $c$ axes perpendicular to the plane of the substrate are observed in the diffraction pattern of figure 3($a$). These oriented domains are surrounded by randomly distributed microdomains (figure 3($c$)). The two electron diffraction patterns confirm that the crystallites have the hexagonal structure of $MoSe_2$. The larger crystals (figure 3($a$)) are well oriented while the smaller ones (figure 3($c$)) are randomly oriented.

Photographs demonstrating the surface morphology after the processes are shown in figure 4. Films obtained by synthesis (figure 4($a$)) are homogeneous and quite granular with a grain size of about 50–100 nm, which confirms the XRD estimation. The surface of the films obtained by tarnishing (figure 4($b$)) is also quite granular with the same average grain sizes but the grains exhibit many very thin needles with lengths of a few hundred nanometres. The grains of these last films look like those obtained by synthesis. As the films obtained by tarnishing are oxidized we can conclude that the needles correspond to $WO_3$.

### *3.2. Optical characterization*

Optical characterization has been performed only on synthesized samples. In order to estimate the indirect band gap of the layers, the variation in the optical absorption with the photon energy $h\nu$ has been calculated. The optical indirect band gap of the $WSe_2$ films was determined to be about 1.05 and 1.25 eV by extrapolating the straight lines of $\alpha$ against $E$ and $\alpha^{1/2}$ against $E$ respectively. Therefore we can conclude that the values obtained for the band gaps of the $WSe_2$ films are of the same order as those of $WSe_2$ single crystals [1] and other thin films [2, 11, 12].

### *3.3. Electrical characterization*

A typical temperature dependence of the resistance between 100 K and 660 K is shown in figure 5. The films are polycrystalline and the conductivity measurements should be interpreted in terms of grain boundary theory [2]. The grain boundary trapping theory assumes the presence of trapping states at the grain boundary, which capture and therefore immobilize free carriers. These charged states at the grain boundary create a depleted region and potential barriers, which oppose the passage of carriers from a grain to the neighbouring ones. It has been shown earlier [2] that, if the model of Lu and co-workers [13] is taken as a starting point to explain our results, the barrier at the grain boundary may be estimated:

$$\sigma \propto T^{-1/2} \exp(-\phi_b/kT) \tag{1}$$

Table 2. Lattice parameters deduced from XRD patterns of synthesized $WSe_2$ layers.

| Samples | $d_{nkl}$ (nm) ±005 (nm) | | | | | | | | | | $c$ (nm) | $a$ (nm) |
|---|---|---|---|---|---|---|---|---|---|---|---|---|
| | 002 | 004 | 100 | 101 | 103 | 006 | 105 | 110 | 008 | 112 | | |
| $V_4$ | 0.653 | — | 0.285 | — | 0.239 | 0.217 | — | 0.165 | 0.162 | 0.160 | 1.301 | 0.329 |
| $V_5$ | 0.651 | — | 0.285 | — | 0.237 | 0.217 | — | 0.165 | 0.163 | — | 1.302 | 0.329 |
| $V_7$ | 0.651 | 0.325 | 0.285 | 0.277 | 0.238 | 0.216 | — | 0.164 | 0.163 | 0.159 | 1.302 | 0.329 |
| $V_{13}$ | 0.651 | — | 0.285 | — | — | 0.217 | — | 0.164 | 0.162 | — | 1.302 | 0.329 |
| $V_{16}$ | 0.651 | 0.324 | 0.284 | 0.279 | 0.238 | 0.217 | 0.192 | 0.165 | 0.162 | — | 1.302 | 0.328 |
| ASTM data No 38-1388 | 0.6494 | 0.3245 | 0.2846 | 0.278 | 0.2378 | 0.21639 | 0.19178 | 0.16229 | 0.16229 | 0.15931 | 1.29825 | 0.32859 |

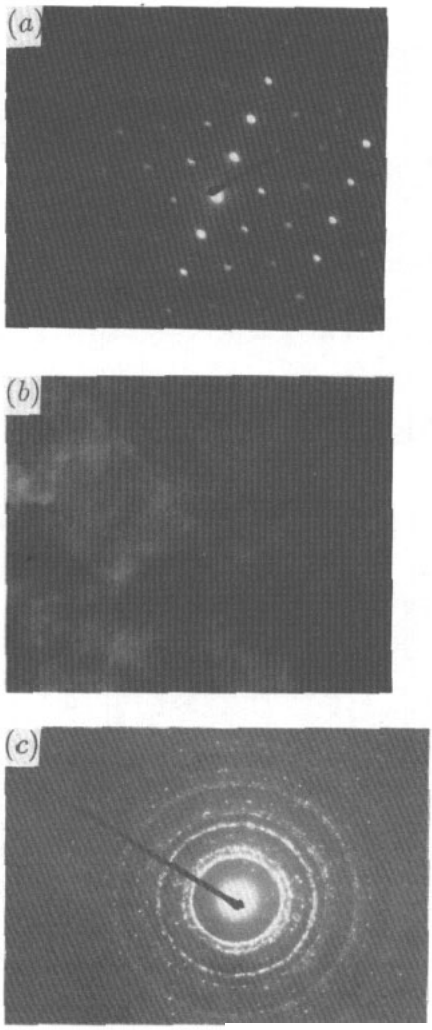


**Figure 3.** (*a*) An electron micrograph of a $WSe_2$ thin film; (*b*) an electron diffraction pattern of a crystal; (*c*) an electron diffraction pattern of randomly oriented microcrystals.

where $\phi_b$ is the barrier height in electronvolts and $k$ the Boltzmann constant.

It can be seen in figure 5 that in the temperature range studied, the conductivity does not follow an Arrhenius dependence. The conductivity of polycrystalline semiconducting thin films depends sensitively on the grain boundaries, that is to say on the potential barriers and space charge regions that are built up around them. Recently a new contribution stated that the Arrhenius plots must be curved due to potential fluctuations at the grain boundaries [14]. The author has shown that the inhomogeneities at the grain barriers due to statistically distributed interface charges result in curved conductivity plots for polycrystalline semiconductors, even if thermal carrier emission across barrier is the only current transport process.

If we introduce potential variations among different boundaries and model the fluctuating

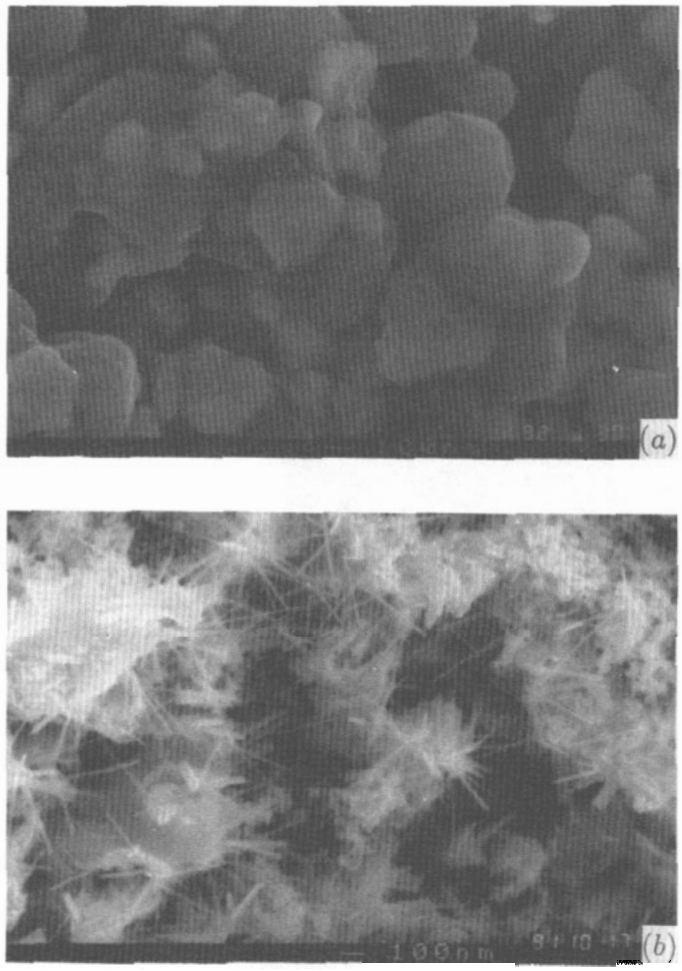


**Figure 4.** The surface morphology of $WSe_2$ layers obtained by (*a*) synthesis ($t_1 = 48$ h, $T_1 = 823$ K) and (*b*) tarnishing ($t = 5$ h, $T = 800$ K).

barrier $\phi$ by a Gaussian distribution:

$$P(\phi) = (1/\sigma_\phi\sqrt{2\pi})e^{-(\bar{\Phi}-\phi)^2/(2\sigma_\phi^2)} \tag{2}$$

with $\bar{\Phi}$ the mean barrier and $\sigma_\phi$ the standard deviation, Werner has shown that the temperature dependent activation energy $E_{act}$ (in figure 5) is given by

$$E_{act}(T) = -k(d/dT^{-1})\ln(\sigma/T) = q(\bar{\Phi}(T=0) - \sigma_\phi^2/(kT/q)). \tag{3}$$

The plots deduced from the derivatives of the curves of figure 5 are shown in figure 6. The corresponding values obtained for $\bar{\Phi}$ and $\sigma_\phi$ are reported in table 3.

Recently we have used this model in the case of $MoSe_2$ thin films [15]. In that paper we have shown that the homogeneity factor $H = \bar{\Phi}(T=0)/\sigma_\phi$ proposed by Werner to qualify the polycrystalline films [14] is not restrictive enough when these films are destined

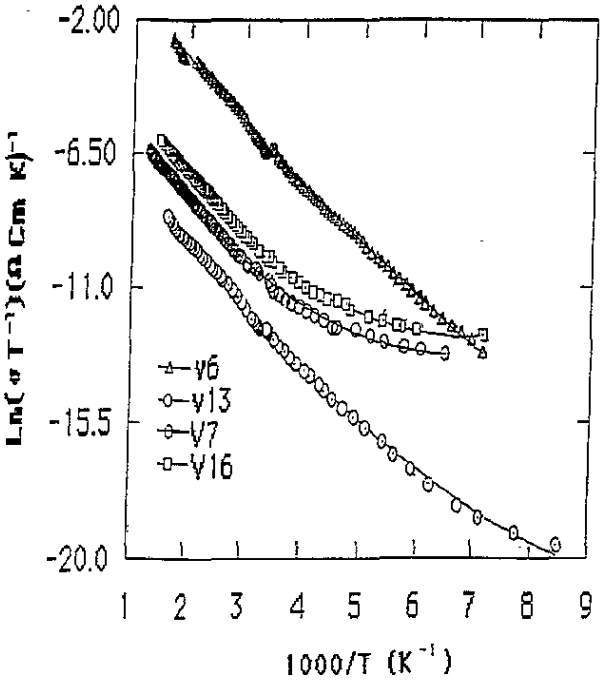


Figure 5. Typical temperature dependences of the electrical resistance of $WSe_2$ thin films.

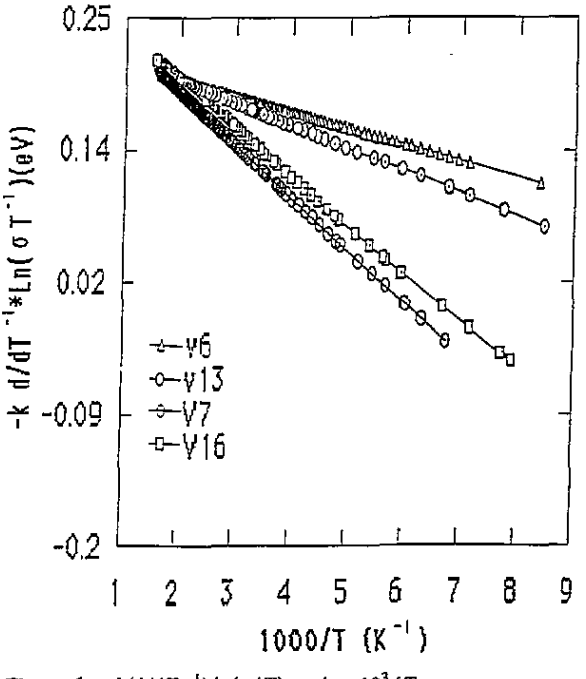


Figure 6. $-k(\mathrm{d}/\mathrm{d}T^{-1})\ln(\sigma/T)$ against $10^3/T$.

**Table 3.** Physical parameters deduced from the plots of figure 6, homogeneity and quality factors.

| | Annealing conditions | | | | | | | |
|---|---|---|---|---|---|---|---|---|
| | $t$ | $T$ | $F_{00l}$ | $\sigma_{300\ K}$ $(\Omega\ cm)^{-1}$ | $q\Phi$ (eV) | $\sigma_\phi$ | $H = \phi/\sigma$ | $Q$ |
| $V_6$ | 48 | 823 | 0.4 | 0.5 | 0.21 | 14 | 15 | 0.34 |
| $V_7$ | 48 | 823 | 0.7 | $1.69 \times 10^{-2}$ | 0.28 | 40 | 6.76 | 0.05 |
| $V_{13}$ | 120 | 823 | 0.7 | $1.3 \times 10^{-3}$ | 0.22 | 20 | 11.7 | 0.006 |
| $V_{16}$ | 120 | 823 | 0.8 | $1.5 \times 10^{-2}$ | 0.28 | 40 | 6.9 | 0.04 |

for photovoltaic applications, where optical and electrical properties are very important. Therefore we have introduced a quality factor $Q$ [15]:

$$Q = \sigma_{tf}/\sigma_{sc} H(1 - |E_{g_{tf}} - E_{g_0}|/E_{g_0}).$$

$\sigma_{tf}$ and $E_{g_{tf}}$ are the thin-film conductivity and optical band gap; $\sigma_{sc}$ and $E_{g_0}$ are the conductivity and optical band gap of the single crystal. (In stoichiometric polycrystalline films we always have $\sigma_{tf} < \sigma_{sc}$). $H$ is the homogeneity factor proposed by Werner such that $H = \bar{\Phi}/\sigma_\phi$. The higher $Q$ is, the higher is the quality of the films.

As can be seen in table 3, there is quite a large scattering of the different values obtained. However it can be seen that, unexpectedly, the films with the best quality factor $Q$ and the best conductivity at room temperature are the ones with the smaller texturing factor $F_{00l}$.

While the calculated barrier height is of the same order as that obtained with the other layers, the standard deviation $\sigma_\phi$ is the smallest. This smaller fluctuation of the barrier height when $F_{00l}$ is small can be understood by using earlier results [16]. We have shown that $WSe_2$ with $F_{00l} = 1$ can be obtained after long annealing (168 h at 823 K). However if the texture of the films increases with annealing time and/or temperature there is also an increase of the number of faults in the layer (pinholes, cracks, etc). Therefore the increase of the fluctuations of the barrier height with $F_{00l}$ corresponds to the increase of the number of defaults in the layers.

If this can explain the differences between the $Q$ factors it is more difficult to understand why the samples $V_6$ and $V_7$, which have undergone identical heat treatments, are different. As discussed earlier [16], the morphology of the layers depends strongly on the Se partial pressure during the annealing. Therefore we can imagine that the volume of the glass tube used was not identical for these two samples (the tube length can varies detectibly from one sample to another).

## 4. Discussion and conclusion

It is clear from previous results, as well as from those shown here, that the films of the transition metal dichalcogenides grow in two preferential orientations, since $F_{00l}$ varies between 0.2 and 0.8 while $F_{hk0}$ varies between 0.4 and 0.1 for the present work. The main factor is the annealing time: when the annealing time increases $F_{hk0}$ decreases, while $F_{00l}$ increases.

The films obtained by synthesis are stoichiometric thin films with gaps almost equal to those of $WSe_2$ single crystals. The resistivity is governed by grain boundary scattering mechanisms. The highest room temperature conductivity of the film with the best quality factor is around 0.5 $\Omega^{-1}$ $cm^{-1}$, which is one order smaller than the conductivity of single

crystals. For economic reasons, the process of synthesis described here has been improved by comparison with the preceding one described in [2]. However the crystalline properties of the texture layers have to be improved in order to decrease the density of defaults and therefore the barrier height fluctuations at the grain boundaries.

The difference of behaviour of samples that have undergone identical heat treatments shows us that a more specific study of the influence of the partial pressure of Se (i.e. the glass tube volume) on the quality of the films has to be carried out.

Films obtained by tarnishing are partly oxidized. This result is quite different from the result obtained by Genut and co-workers [4], who obtain, by tarnishing, $WS_2$ layers free from oxide. The main difference between the two processes used is the chalcogen vapour source. Genut and co-workers used $H_2S$ while we used Se powder. We believe that the chalcogen pressure in the reactor is higher in the former case than in the latter; therefore the reaction is slower in our case. We think that contamination of the slowly growing $WSe_2$ films is very important. This is due to O contamination during the reaction.

Therefore, it may be necessary to use $H_2Se$ as the Se source to improve the quality of the $WSe_2$ films obtained by tarnishing.

## References


[1] Tributsch H 1977 *Ber. Bunsenges. Phys. Chem.* **84** 361
[2] Pouzet J, Bernède J C, Khelil A, Essaidi H and Benhida S 1992 *Thin Solid Films* **208** 252
[3] Curran J S, Nguyen Du, Philippe R and Stremsdoerfer G 1986 *Thin Solid Films* **144** 117
[4] Genut M, Margulis L, Hodes G and Tenne R 1992 *Thin Solid Films* **217** 91
[5] Kaeble E F 1967 *Handbook of X-rays* (New York: McGraw-Hill)
[6] Klug H P and Allexander L E 1954 *X-ray Diffraction Procedures* (New York: Wiley)
[7] Janda M and Kubovy A 1976 *Phys. Status Solidi* a **35** 391
[8] Beal A R, Liang W Y and Hughes H P 1976 *J. Phys. C: Solid State Phys.* **9** 2449
[9] Bernède J C, Mallouky A and Pouzet J 1988 *Mater. Chem. Phys.* **20** 201
[10] Goldberg A M, Beal A R, Levy F A and Davis E A 1975 *Phil. Mag.* **32** 367
[11] Cabrera C R and Abruna H D 1985 *J. Phys. Chem.* **89** 1279
[12] Jager-Waldau A and Bucher E 1991 *Thin Solid Films* **200** 157
[13] Lu C C, Luan C Y and Meindl J D 1981 *IEEE Trans. Electron Devices* **ED-28** 818
[14] Werner J H 1994 *Polycrystalline Semiconductors III. Physics and Technology, Solid State Phenomena* vol XXX, ed H P Strunk, J H Werner, B Fortin and O Bonnaud (Zurich: Trans Tech)
[15] Bernède J C, Pouzet J, Le Ny R and Ben Nasrallah T 1994 *J. Physique III* **4** 677
[16] Benhida S, Bernède J C, Pouzet J and Barreau A 1993 *Thin Solid Films* **224** 39